Feb. 20, 1985

The Multi-Telescope Component of the Proposed mm Array

R.M. Hjellming

I. INTRODUCTION

The most compact configuration for the proposed NRAO mm array facility is 25 m. in diameter. Because this is difficult to achieve with the 10 m. antennas of the larger configurations of the mm array, it has been proposed (mm Array Memos 1 and 10) that a number of smaller antennas, 3-5 m. in diameter, be mounted upon a structure that will, itself, be pointed at sources being observed. The purpose of this memo is to present preliminary results for some of the properties of configurations of this type.

The aperture synthesis characteristics of a group of radio telescopes mounted upon a structure which moves with respect to the surface of the earth are different from those of telescope systems with elements fixed on the surface of the earth. Therefore we must derive the special equations for the u-v plane under these circumstances.

There are two types of multi-telescope systems that will be considered: (1) telescopes mounted on a structure which tracks (in altitude and azimuth) an observed source in the sense that the mounting surface is always peripindicular to the line of sight to the source; and (2) telescopes mounted on a structure which tracks a source by rotating in azimuth while the individual telescope elements move in elevation to follow the source declination. The former structure corresponds to mounting antennas on the surface of a normal Alt-Az tracking antenna, as discussed in mm Array Memo 10 and sketched in Figure 1; we will call this type of array a "tracking surface array". The second type of M-T structure is a different combination of the two axes of motion. The first axis is azimuth-rotation around a set of tracks (as with the original Jansky and Reber antennas, and the Bonn 100 m. telescope), while the other axis is tracking in elevation for each radio telescope on the rotating structure. We will call this type of array an "azimuth-rotation" array. Figure 2 shows schematic versions of possible two-dimensional (inclined plane) and three-dimensional structures of this type.

II. GEOMETRY AND THE U-V EQUATIONS

1. Tracking Surface Arrays

Let us assume that we have n antennas of diameter d mounted on a structure, such as the surface of an Alt-Az tracking paraboloid, which maintains an orientation perpindicular to the line of sight to a source while the source is being tracked. Let the x-y-z coordinate system have an origin at

the center of the tracking surface, with the y- and z-coordinates perpindicular to the direction to the source, the y-axis being horizontal, and the z-axis pointing "up" but confined to the plane of the tracking surface. The parallactic angle, ϕ_p, is the angle between the z-axis and the local meridian with hour angle H. Figures 3a and 3b illustrate the geometry of this situation. Describing the location of the n-th antenna on the tracking surface by coordinates (y_n, z_n), the location of the n-th antenna in the sky-oriented u-v coordinate system is obtained by clockwise (for $H < 0$) or counter-clockwise (for $H > 0$) rotation by the parallactic angle (ϕ_p), that is

$$u_n = y_n \cos p + y_n \sin p \tag{1a}$$

and

$$v_n = -y_n \sin p + y_n \cos p \tag{1b}$$

where

$$p = -\phi_p \quad \text{if } H > 0 \tag{2a}$$

and

$$p = +\phi_p \quad \text{if } H < 0. \tag{2b}$$

As we will derive shortly,

$$\phi_p = \tan^{-1}[(\cos \phi \sin H)/(\sin \phi \cos \delta - \cos \phi \sin \delta \cos H)] \tag{3}$$

where

H = hour angle of the source with respect to the local meridian,

δ = declination of the source being tracked, and

ϕ = geocentric latitude of the instrument.

Equations (1)-(3) indicate that the projections of baseline pairs of elements on a tracking surface array will be circles in the u-v plane with rotation with respect to the zenith by the angle p. This means that the tracking range in the u-v plane is constrained by the limits on parallactic angle, which differs for each declination. In Figure 4 we show both a geometry figure and a plot of parallactic angle, ϕ_p, as a function of H, taken from the "Introduction to the VLA" . Figure 3a (and 3b) and Figure 4a are related in that sense that the y-axes are identical, although the z-axes differ by a rotation of $h = \pi/2 - \zeta$ in the x-z plane (local meridian).

Because they are critical to the equations simulating the mm array, let us derive the equations relating latitude, declination, and hour angle to azimuth, altitude, and parallactic angle. This will indicate assumptions used in deriving the ensuing equations.

A = azimuth (location of x-axis with respect to the local meridian) where 0 is North and 90° is East,

h = altitude of source above the horizon,

and

ζ = zenith angle of source (= $\pi/2$ - h).

The following shows the spherical triangle involved in the transformation between the Alt-Az and sky coordinate systems.

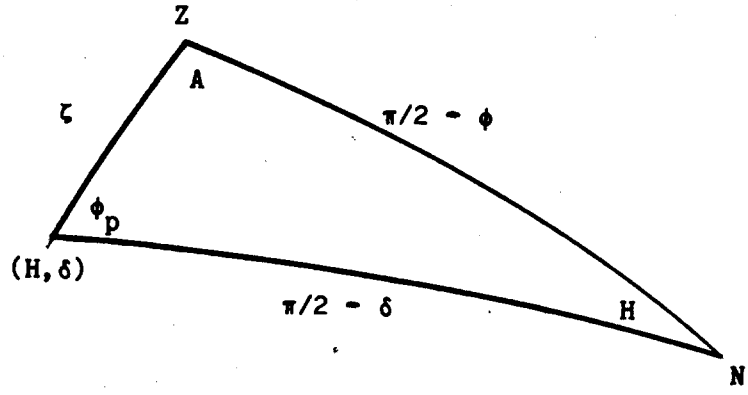

For this spherical triangle we will utilize the Law of Sines

$$\sin A / \sin(\pi/2 - \delta) = \sin H / \sin \zeta = \sin \phi_p / \sin(\pi/2 - \phi) \qquad (4)$$

and various forms of the Law of Cosines, of which one is

$$\begin{aligned} \cos \zeta = \sin h &= \cos(\pi/2-\delta)\cos(\pi/2-\phi) + \sin(\pi/2-\delta)\sin(\pi/2-\phi)\cos H \\ &= \sin\delta \sin\phi + \cos\delta \cos\phi \cos H \end{aligned} \qquad (5)$$

from which one derives ζ (or h). Note that we have used (and will frequently use) the identities $\sin(\pi/2-\theta) = \cos\theta$ and $\cos(\pi/2-\theta) = \sin\theta$. The Law of Cosines for another combination of angles is

$$\cos(\pi/2-\phi) = \cos\zeta \cos(\pi/2-\delta) + \sin\zeta \sin(\pi/2-\delta)\cos\phi_p \quad . \qquad (6)$$

Equation (6) and the part of Equation (4) involving ϕ_p and H can be used to derive the equation for parallactic angle (ϕ_p):

$$\phi_p = \tan^{-1}[(\cos\phi \sin H)/(\sin\phi \cos\delta - \cos\phi \sin\delta \cos H)] \quad (3)$$

The third possible version of the Law of Cosines for this spherical triangle is

$$\cos(\pi/2-\delta) = \cos\zeta \cos(\pi/2-\phi) + \sin\zeta \sin(\pi/2-\phi) \cos A \quad , \quad (7)$$

thus Equation (7), and the part of Equation (4) involving A and H, can be used to derive the following equation for azimuth:

$$A = \tan^{-1}(\sin H \cos\delta)/(\sin\delta \cos\phi - \sin\phi \cos\delta \cos H) \quad . \quad (8)$$

2. Azimuth-Rotation Arrays

The u-v coordinates for antenna pairs on an azimuth-rotation array are slightly different. For this case let us use the x-y-z coordinate system exactly as defined in Figures 3c, 3d and 4a. The z-axis points to the zenith while the y-axis parallel to the ground. With an antenna at a location (x_n, y_n, z_n) one can define an angle

$$\psi_{nm} = \tan^{-1}[(z_m - z_n)/(x_m - x_n) \quad (9)$$

(cf. Figure 3c) which is the "tilt" angle the n-th and m-th antennas make with repect to the ground. As seen in Figure 3c, one can define an angle ε_{nm} which is the angle (in the x-z plane) that one needs to rotate the line between antennas n and m to make their baseline perpindicular to the line pointing to the source. One therefore has

$$\varepsilon_{nm} = \zeta - \psi_{nm} = \zeta - \tan^{-1}[(z_m - z_n)/(x_m - x_n) \quad . \quad (10)$$

The u-v equations for this geometry are then

$$u_{nm} = (y_n - y_m)\cos p + \Delta_{nm} \sin p \quad (11a)$$

and

$$v_{nm} = -(y_n - y_m)\sin p + \Delta_{nm} \cos p \quad (11b)$$

where

$$\Delta_{nm} = [(x_n - x_m)^2 + (z_n - z_m)^2])^{1/2} \cos \varepsilon_{nm} \quad . \qquad (11c)$$

Equation (11) for azimuth-rotation arrays is an obvious extension of Equations (1)-(3) for the full tracking arrays.

III. TWO VERSIONS OF FULL TRACKING ARRAYS

Figures 5a and 5c show two possible versions of a full tracking array where 21 antennas are mounted at the indicated locations on a surface 25 meters in diameter. Figure 5a (TRACK21) is symmetric in the sense that the small antennas are located on an evenly spaced grid, whereas in Figure 5c (TRACKM21) the inner antennas are re-arranged slightly in location in order to increase the number of different spacings between antennas, and the y- and z- spacing interval differ by 10%. In this section let us discuss the aperture synthesis properties of these two full tracking arrays.

In mm Array memo 21 one of the major differences between different types of configurations of large antennas was the radial distribution of the number of data points in the u-v plane. Figures 5b and 5d show this distribution for the symmetric and non-symmetric full tracking arrays, in the form of plots of the number of data points in equal thickness rings as a function of u-v radius for a 12 hour observation of a source at 60° declination. In these cases there is no significant difference in the shape of this distribution.

1. A Symmetric and Non-symmetric Full Tracking Array

Figure 6 shows the u-v coverage and beam profiles for three different type of observations with the symmetric full tracking array with small antennas arranged as shown in Figure 5a (TRACK21). The left three sub-figures are (1) the u-v coverage, (2) the N-S beam profile for natural weighting of the data, and (3) the N-S beam profile for uniform weighting of the data, all for the case of a 12 hour observation at a declination of 60°. The middle three sub-figures provide the same information for a 10 minute snap-shot of the same source observed at transit, and the right three sub-figures give the same information for a 6 hour observation at -30° declination. For the 12 hour observation there is a great deal of redundant sampling of data in the same rings in the u-v plane. For the 10 minute snapshop only a small part of each circle is sampled. For the -30° observation of 6 hours the circles are not complete because of the limited range of parallactic angle. For all beam profiles vertical lines appear in the figures at the locations of the antenna HPBW for an assumed diameter of 4 meters.

The beam profiles for uniform weighting for all three cases in Figure 6 are very similar, with only slightly poorer characteristics for the ten minute snapshot. This is because nearly all cells in the the u-v plane (gridded for two points per synthesized beam) that can be filled with data are sampled for all cases, which is a consequence of the 17 X 17 array of cells for 4m antennas on a 25m structure. However, the naturally weighted beams are slightly less desireable for the shorter observations because of the large circular gaps in

the u-v plane.

The qualitative information in Figure 6 can be supplemented with various quantitative measures that we will find useful in comparing arrays. In Table 1 we list the following: a name for the array; the intervals (in meters) between antennas in y- and z-coordinates; the hour angle range of continuous observation; the declination, δ; synthesized HPBW for natural ($\theta_{B,na}$) and uniform ($\theta_{B,un}$) weighting divided by the wavelength in mm (λ_{mm}); the fraction of potentially fillable cells that contain data; the number of occupied cells in the 17 X 17 grid, N_{occ}; the mean number of data points in each occupied cell, N_M; the harmonic mean number of data points in each occupied cell, N_{HM}; the rms sidelobe levels for natural and uniform weighting using the formulas discussed in mm Array memo numbers 18 and 20; the rms map noise in mJy for natural and uniform weighting, assuming a system temperature of 100°K, an antenna aperture efficiency of 0.5, bandwidths of 1 GHz or 0.1 MHz, and 21 4m antennas; and finally, the rms brightness temperatures derived from the previously listed rms map noise and synthesized HPBW, in units of mK for 1 GHz bandwidth and units of K for 0.1MHz bandwidth. The synthesized HPBW, θ_B, used in these and other tables in this memo were derived by numerically integrated the beam solid angle of the central beam and converting this to the HPBW of a Gaussian with the same beam solid angle. These results for the symmetric (Fig. 5a, TRACK21) and non-symmetric (Fig. 5c, TRACKM21) full tracking arrays three different observing situations are listed in Table 1.

Figure 7 gives the information on the non-symmetric full tracking array shown in Fig. 5c (TRACKM21) which is equivalent to that in Figure 6 for the TRACK21 symmetric array.

2. Conclusions about the Desireable Full Tracking Array

The more even u-v plane coverage of the non-symmetric full tracking array is qualitative indication of the improved parameters of that array. The core of the synthesized beam for the 10 minute snapshot and natural weighting is better defined and leads to better numerical parameters in most cases. The sole exceptions are the results for surface brightness sensitivity where the "fatter" core beam of the symmetric array leads to apparently lower rms noise in surface brightness. However, the more ideal beam is more desirable since increased beam width can always be attained with tapering. The more random locations of antennas eliminate many of the gaps in the u-v coverage for the -30° case that are due to the ±40° limitation on parallactic angle for this declination.

Table 1

Parameters for the Symmetric (TRACK21)
and Non-Symmetric (TRACKM21) Full Tracking Arrays

Name	TRACK21	TRACK21	TRACK21	TRACKM21	TRACKM21	TRACKM21
M-T Spacing	4.3,4.3	4.3,4.3	4.3,4.3	4.7,4.3	4.7,4.3	4.7,4.3
H Range	$-6^h,6^h$	$0^h,0.17^h$	$-3^h,3^h$	$-6^h,6^h$	$0^h,0.17^h$	$-3^h,3^h$
δ	60^o	60^o	-30^o	60^o	60^o	-30^o
$\theta_{B,na}/\lambda_{mm}$	6.61"	7.39"	6.54"	7.07"	7.06"	7.05"
$\theta_{B,un}/\lambda_{mm}$	4.63"	5.24"	4.83"	4.98"	5.76"	5.39"
N_{occ}/N_{theo}	0.83	0.30	0.74	0.79	0.50	0.65
N_{occ}	188	67	169	169	113	148
N_M	161	6.3	89	179	3.7	102
N_{HM}	24	3.7	24	45	2.4	30
Sidelobe σ_{na}	0.105	0.149	0.105	0.101	0.114	0.102
Sidelobe σ_{un}	0.073	0.122	0.077	0.077	0.094	0.082
Noise σ_{na}(1GHz)	0.40 mJy	3.42 mJy	0.57 mJy	0.40 mJy	3.42 mJy	0.57 mJy
Noise σ_{un}(1GHz)	1.04 mJy	4.42 mJy	1.09 mJy	0.81 mJy	4.27 mJy	1.04 mJy
Noise σ_{na}(0.1GHz)	40 mJy	342 mJy	57 mJy	40 mJy	342 mJy	57 mJy
Noise σ_{un}(0.1GHz)	104 mJy	442 mJy	109 mJy	81 mJy	427 mJy	104 mJy
$T_{b,na}$(rms,1GHz)	0.12 mK	0.85 mK	0.18 mK	0.11 mK	0.93 mK	0.16 mK
$T_{b,un}$(rms,1GHz)	0.66 mK	2.17 mK	0.64 mK	0.44 mK	1.75 mK	0.49 mK
$T_{b,na}$(rms,0.1GHz)	0.012 K	0.085 K	0.018 K	0.011 K	0.093 K	0.016 K
$T_{b,un}$(rms,0.1GHz)	0.066 K	0.217 K	0.064 K	0.044 K	0.175 K	0.049 K

IV. TWO VERSIONS OF TWO-DIMENSIONAL (INCLINED PLANE) AZIMUTH-ROTATION ARRAYS

The azimuth-rotation arrays that one can design have many similarities and some differences when compared to the full tracking arrays. Let us first discuss two versions of azimuth-rotation arrays where the antennas are located on a two-dimensional surface or inclined plane (cf. Figure 2a).

Figure 8 shows the antenna locations (projected on the x-y plane) and radial distributions of data points in the u-v plane for the symmetric and non-symmetric versions of inclined plane arrays labeled ROTBL21 and MROTBL21, respectively (names related to a visual impression of these arrays as "rotating bleachers" arrays). As before for the full tracking arrays, the symmetry vs. non-symmetry makes no significant difference in the radial distribution of data points in the u-v plane as seen from Figures 8b and 8d.

The u-v plane, natural weight beam, and uniform weight beams for a 12 hour observations of a source at 60° declination, a 10 minute snapshot at the same declination, and a 6 hour observations a -30° declination are shown in Figure 9 for the symmetric ROTBL21 azimuth-rotation array and in Figure 10 for the non-symmetric MROTBL21 array. The parameters listed in tabular form for the full tracking arrays are presented for these azimuth-rotation arrays in Table 2. As before, some non-symmetry spreads the data more evenly in the u-v plane. However, most importantly, the non-symmetric version avoids the hideous secondary sidelobes at the edge of the antenna beam that are due to the "grid interval" for the symmetric case. These were less important for the full tracking symmetric array because the "grid interval" was a factor of two less in each dimension because of the "diamond" grid adopted, rather than the square grid used for ROTBL21. The point of all this is that an appropriate degree of randomization is very helpful in improving both u-v plane and instantaneous beam characteristics. However, for longer observations all cases give reasonable results because of the nearly complete sampling of the u-v plane that is then achieved.

Close perusal of Tables 1 and 2 together with Figures 5-10 indicate only minor differences between the observational properties of the non-symmetric full tracking and azimuth-rotation arrays. The full tracking array is slightly better because a large number of circular segments has more predictable properties than the declination-dependent tracks of the azimuth rotation arrays which have a geometry dependent cosine factor (cf. Equation 11) forshortening the projection of the x-z-plane on the sky. However, the azimuth-rotation arrays may have significantly better cost and differential stability characteristics because one is placing a squat inertial mass close to the ground. Thus the choice between arrays of this type will probably made on structural analysis considerations that require detailed computations as part of the pre-design phase for antenna structures.

Table 2

Parameters for a Symmetric (ROTBL21)
and Non-Symmetric (MROTBL21) Azimuth-Rotation Arrays

Name	ROTBL21	ROTBL21	ROTBL21	MROTBL21	MROTBL21	MROTBL21
M-T Spacing	4.3,4.7	4.3,4.7	4.3,4.7	4.3,4.7	4.3,4.7	4.3,4.7
H Range	$-6^h,6^h$	$0^h,0.17^h$	$-3^h,3^h$	$-6^h,6^h$	$0^h,0.17^h$	$-3^h,3^h$
δ	60^o	60^o	-30^o	60^o	60^o	-30^o
$\theta_{B,na}/\lambda_{mm}$	7.34"	8.00"	7.62"	6.99"	6.82"	7.04"
$\theta_{B,un}/\lambda_{mm}$	4.93"	5.37"	5.32"	4.43"	5.33"	5.02"
N_{occ}/N_{theo}	0.74	0.18	0.41	0.96	0.30	0.53
N_{occ}	168	41	94	217	69	121
N_M	180	10	161	139	6.1	125
N_{HM}	25	3.9	16	13	3.0	18
Sidelobe σ_{na}	0.115	0.209	0.157	0.102	0.149	0.135
Sidelobe σ_{un}	0.077	0.156	0.103	0.068	0.120	0.091
Noise σ_{na}(1GHz)	0.40 mJy	3.42 mJy	0.57 mJy	0.40 mJy	3.42 mJy	0.57 mJy
Noise σ_{un}(1GHz)	1.09 mJy	5.53 mJy	1.81 mJy	1.31 mJy	4.85 mJy	1.52 mJy
Noise σ_{na}(0.1GHz)	40 mJy	342 mJy	57 mJy	40 mJy	342 mJy	57 mJy
Noise σ_{un}(0.1GHz)	109 mJy	553 mJy	181 mJy	131 mJy	485 mJy	152 mJy
$T_{b,na}$(rms,1GHz)	0.10 mK	0.73 mK	0.13 mK	0.11 mK	1.00 mK	0.16 mK
$T_{b,un}$(rms,1GHz)	0.61 mK	2.61 mK	0.87 mK	0.91 mK	2.32 mK	0.82 mK
$T_{b,na}$(rms,0.1GHz)	0.010 K	0.073 K	0.013 K	0.011 K	0.10 K	0.016 K
$T_{b,un}$(rms,0.1GHz)	0.061 K	0.261 K	0.087 K	0.091 K	0.232 K	0.082 K

V. ONE VERSION OF A THREE-DIMENSIONAL AZIMUTH-ROTATION ARRAY

In Figure 2b we showed a sketch of one way to place 21 small antennas on an azimuth-rotation structure, where the antennas are distributed in three dimensions. This reduces the size, volume, cross-section, etc. for the structure and provides a base geometry that matches the railroad tracks that one provides for support of any rotating structure. In Figure 11a we show one scheme of locations of 21 antennas on such a structure, with antenna positions shown as projected on the x-y plane. This array is designated ROTHIV21. It has u-v plane density characteristics as shown in Figure 11b - again not significantly different from that of any array discussed in this memo.

Figure 12 shows the u-v plane, natural weighted beam, and uniform weighted beam for the ROTHIV21 array and the same observing situations discussed for the other arrays. Table 3 summarizes the same numerical parameters for this three-dimensional azimuth-rotation array.

The ROHIV21 array is not significantly poorer than the other non-symmetric arrays, and can be significantly improved by more small adjustments in antenna locations to remove some of the sidelobes appearing at the antenna HPBW points.

VI. CONCLUSIONS

We have evaluated the characteristics of a few examples of full tracking arrays, two-dimensional azimuth-rotation arrays, and a three-dimensional azimuth-rotation array. All can obviously be made to have the needed desireable characteristics if suffient non-symmetry is introduced to avoid the clumping in the u-v plane that leads to undesirable sidelobes, particularly for the short snapshot observations that are very important to the mosaicing schemes being suggested for mapping regions much larger that the antenna field of view. The non-symmetric arrays that we have discussed, and many other non-symmetric arrays based upon the same principles, are capable of filling nearly all of the cells in the u-v plane that are needed to satisfy sampling theory, even for short snapshots.

If the costs and structural stability characteristic of these three types of arrays are all comparable, the non-symmetric full tracking array has the best overall characteristics (to a slight degree) and hence would be preferable. However, if either two- or three-dimensional azimuth rotation arrays turn out to have lower costs, or better characteristics of stability against thermal, wind, or gravitational effects, then these cost or stability characteristics can be the main basis for choosing amongst these arrays. We have not experimented with any but a small number of potential antenna locations on such structures because we intended to demonstrate only adequacy. Further work on locations of small antennas on structures can proceed once we know: (1) if we want a multi-telescope array of roughly these characteristics; (2) which structures are most cost-effective; (3) and which structures have the best stability against deformation by gravitation, wind, and thermal effects.

Table 3

Parameters for a Three-Dimensional Azimuth-Rotation Array (ROTHIV21)

H Range	$-6^h,6^h$	$0^h,0.17^h$	$-3^h,3^h$
δ	60^o	60^o	-30^o
$\theta_{B,na}/\lambda_{mm}$	6.20"	6.47"	6.73"
$\theta_{B,un}/\lambda_{mm}$	4.57"	5.18"	5.21"
N_{occ}/N_{theo}	0.90	0.34	0.56
N_{occ}	205	77	126
N_M	148	5.5	120
N_{HM}	22	3.2	21
Sidelobe σ_{na}	0.098	0.151	0.138
Sidelobe σ_{un}	0.070	0.114	0.089
Noise σ_{na}(1GHz)	0.40 mJy	3.42 mJy	0.57 mJy
Noise σ_{un}(1GHz)	1.05 mJy	4.47 mJy	1.35 mJy
Noise σ_{na}(0.1GHz)	40 mJy	342 mJy	57 mJy
Noise σ_{un}(0.1GHz)	105 mJy	447 mJy	135 mJy
$T_{b,na}$(rms,1GHz)	0.13 mK	1.21 mK	0.17 mK
$T_{b,un}$(rms,1GHz)	0.68 mK	2.26 mK	0.68 mK
$T_{b,na}$(rms,0.1GHz)	0.013 K	0.12 K	0.017 K
$T_{b,un}$(rms,0.1GHz)	0.068 K	0.23 K	0.068 K

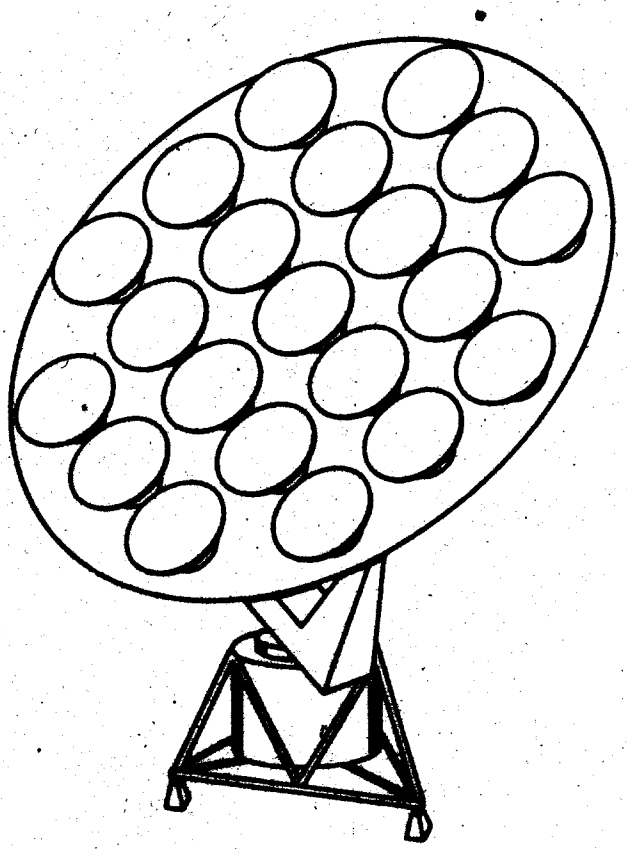

Fig. 1 - Schematic drawing of a full tracking array with 21 small antennas on a large surface.

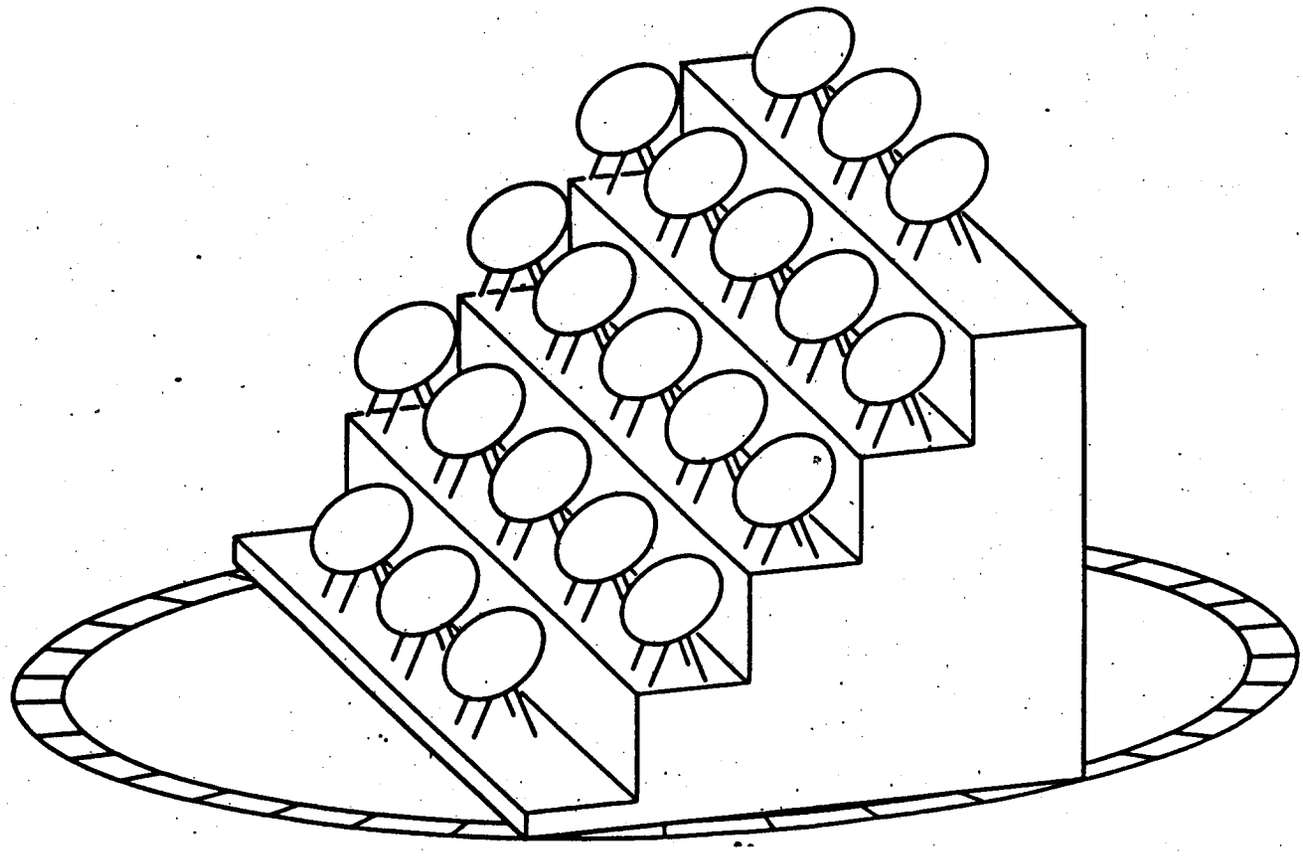

Fig. 2a - Schematic of one version of a two-dimensional (inclined plane) Azimuth-Rotation Array of 21 antennas.

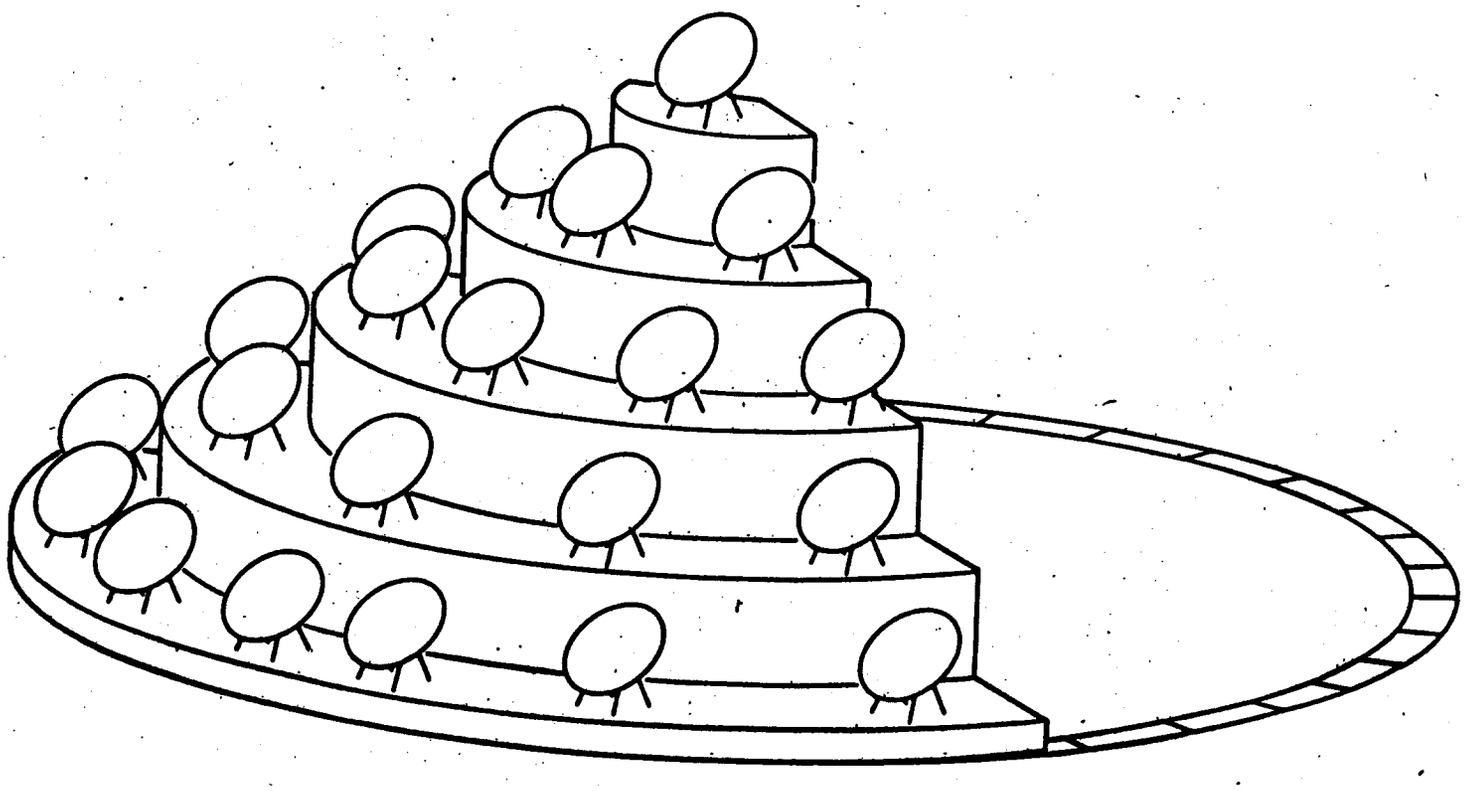

Fig. 2B - Schematic of one version of a three-dimensional Azimuth-Rotation Array.

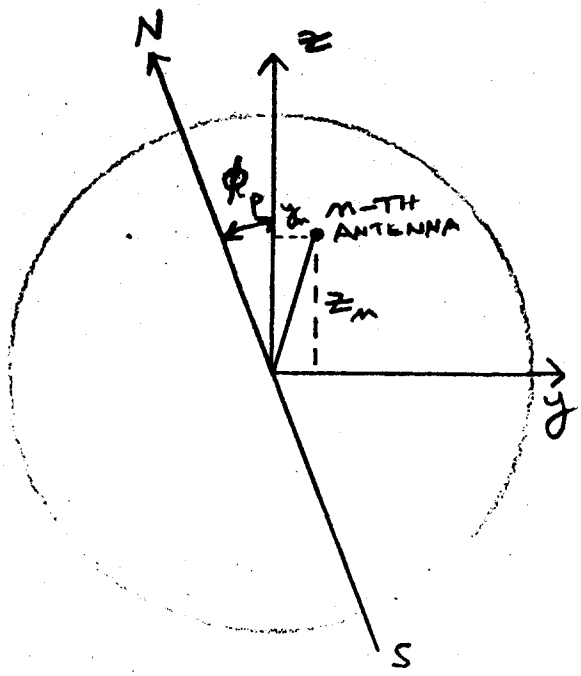

Fig. 3a

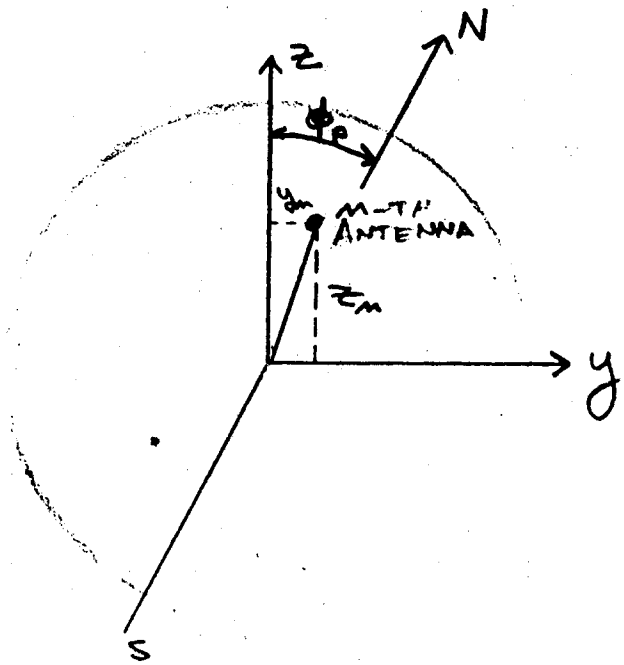

Fig. 3b

Geometry of the n-th antenna mounted on the surface of a full tracking array structure, showing the relation between the antenna coordinates (y_n, z_n), parallactic angle, and the intersection with the local meridian for (a) positive hour angles and (b) negative hour angles.

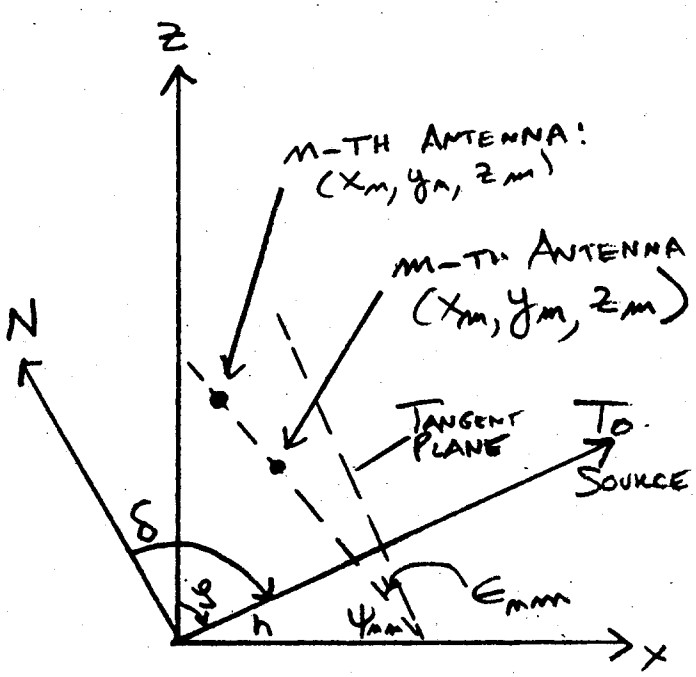

Fig. 3c - Geometry of the n-th and m-th antennas on an Azimuth-Rotation structure, showing relation to the x-y-z coordinate system as seen in x-z cross-section.

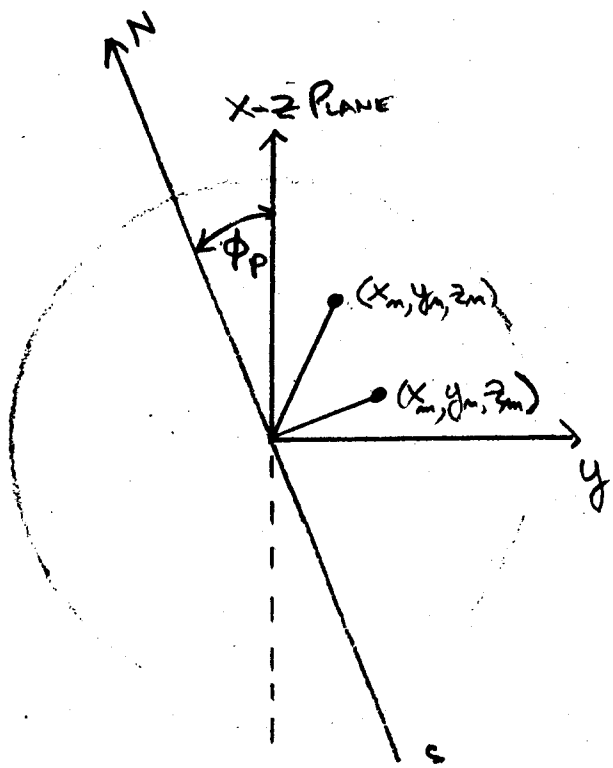

Fig. 3d - Geometry of the n-th and m-th antennas on an Azimuth-Rotation structure, showing the relation between the y-z plane, parallactic angle, and the local meridian.

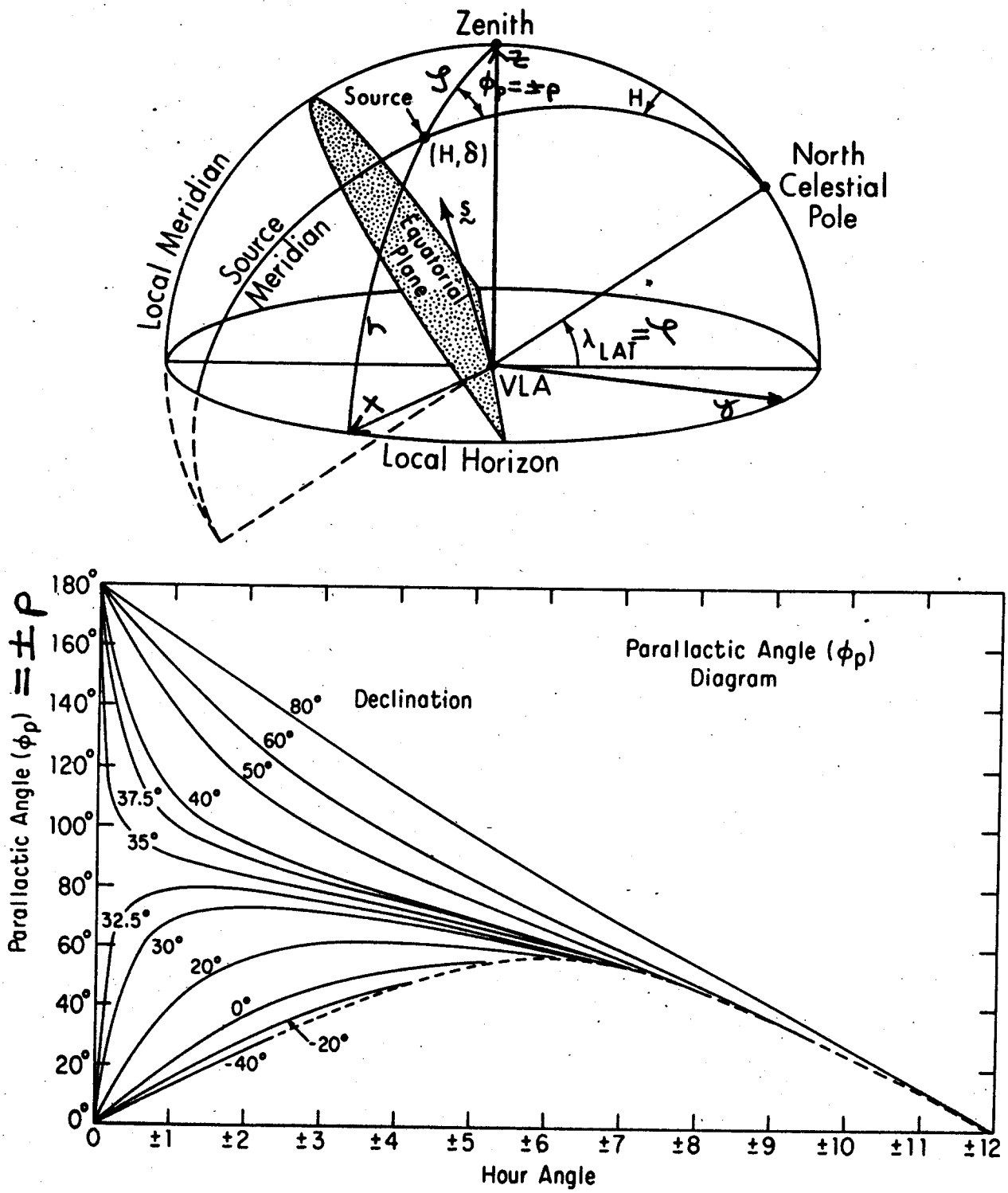

Fig. 4 - (a) The geometric relation between the Alt-Az (x-y-z) coordinate system and various parameters; and (b) the plot of parallactic angle as a function of hour angle.

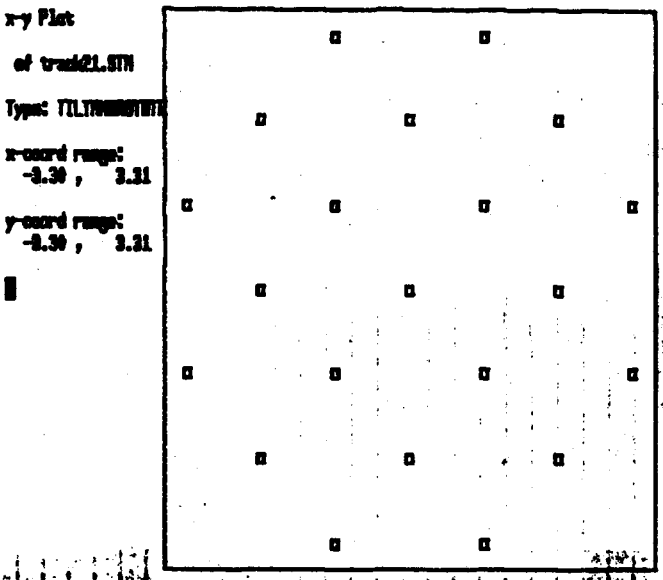

Fig. 5a - Location of antennas on a surface, making a "gridded" version of a full-tracking array (TRACK21).

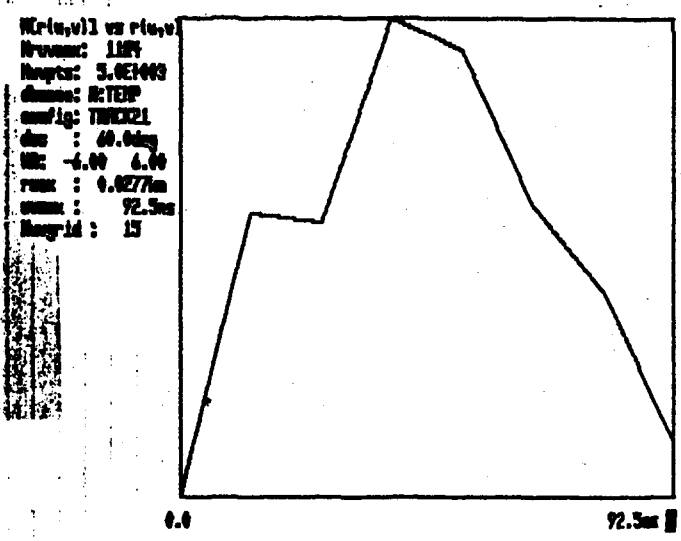

Fig. 5b - The distribution of data points in equal thickness rings in the u-v place for a 60°, 12 hour observation with TRACK21.

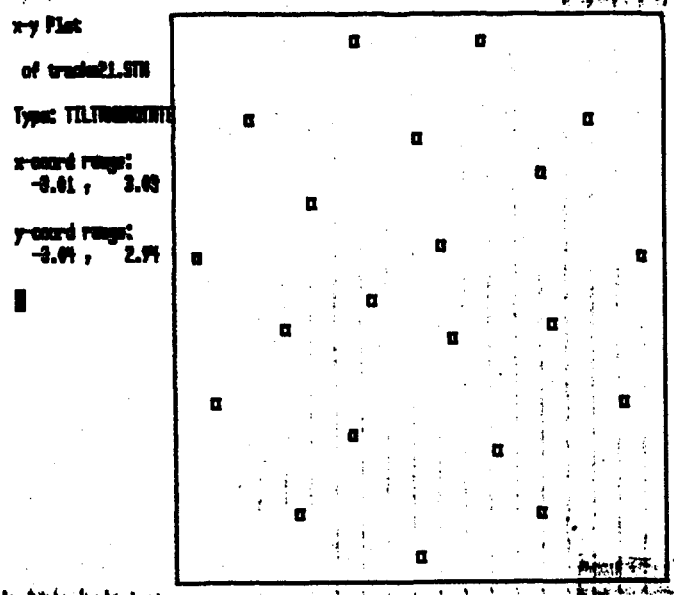

Fig. 5c - Location of antennas for the tracking surface array TRACKM21, where the inner antennas have been slightly "randomized" in location.

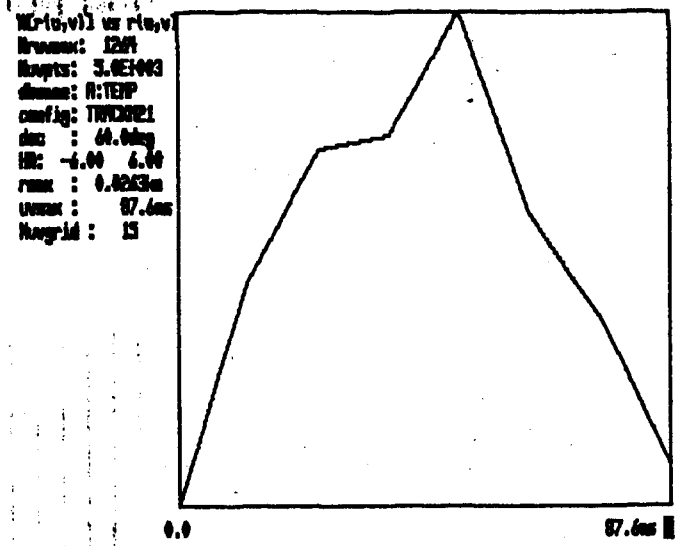

Fig. 5d - The distribution of data points in equal thickness rings in the u-v plane for a 60°, 12 hour observation with TRACKM21.

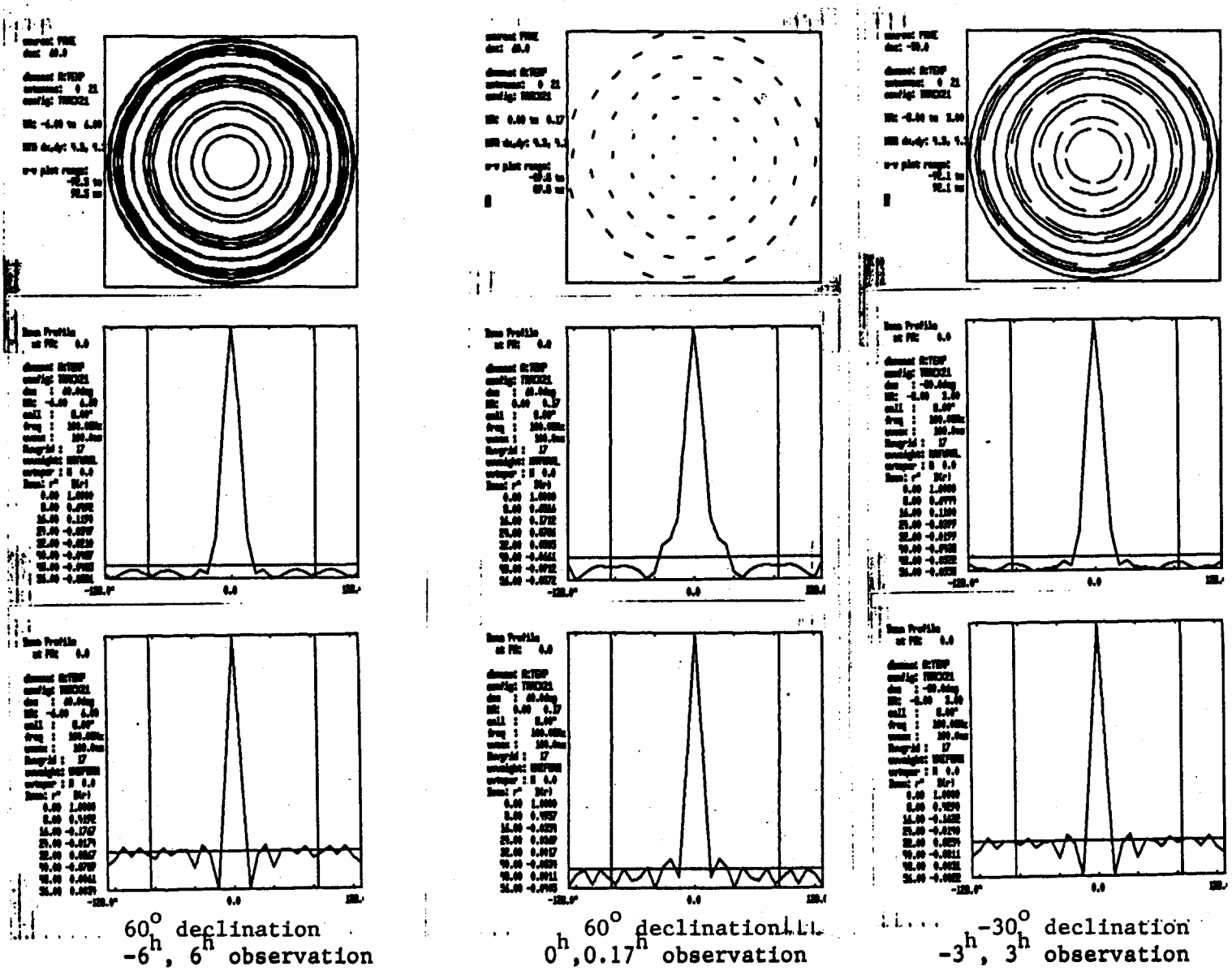

Fig. 6 - The u-v plane coverage, and natural and uniform weighted beam profiles for the tracking surface array TRACK21.

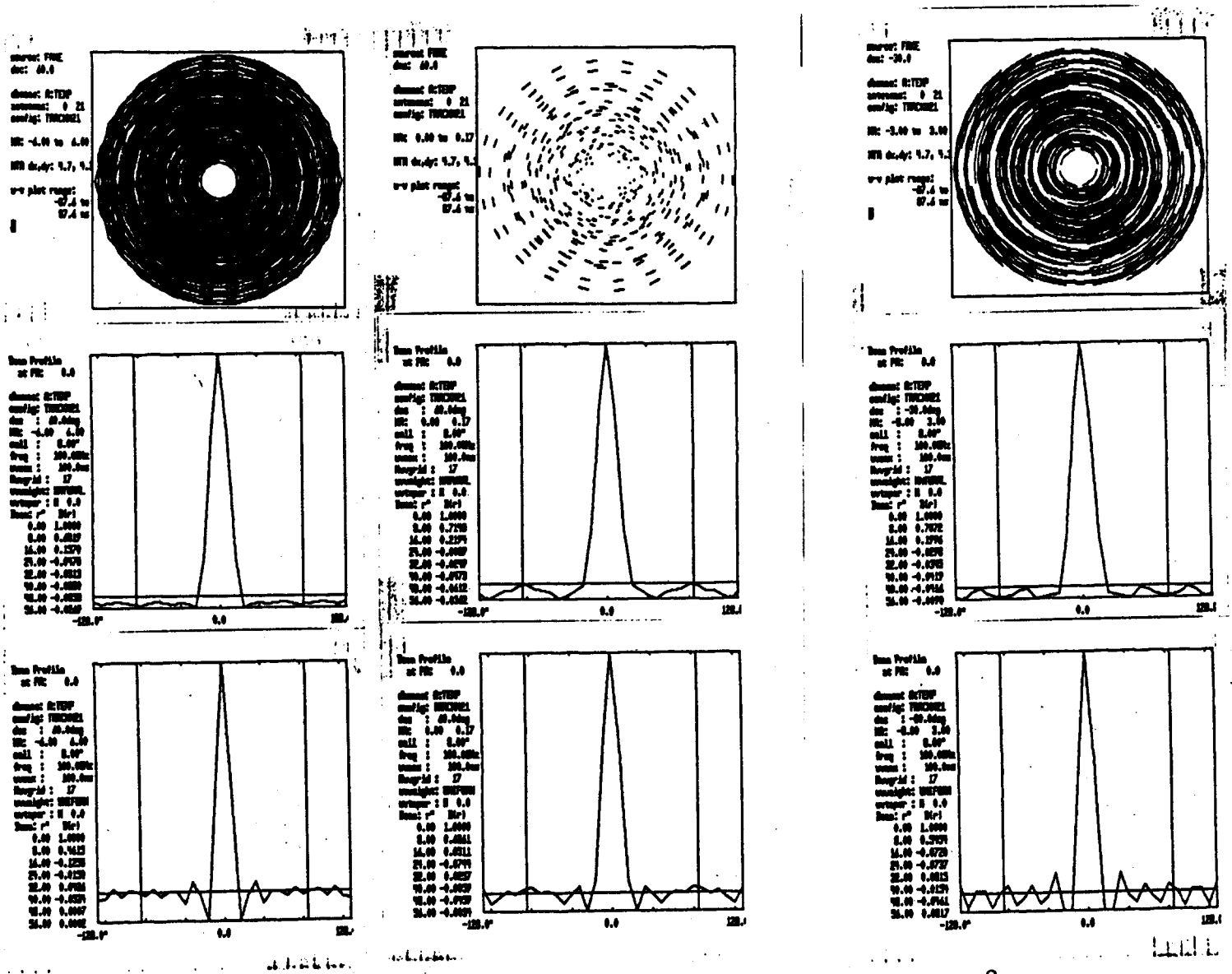

60° declination
-6h, 6h observation

60° declination
0h, 0.17h observation

-30° declination
-3h, 3h observation

Fig. 7 - The u-v plane coverage, and natural and uniform weighted beam profiles for three observing situations for the tracking surface array TRACKM21.

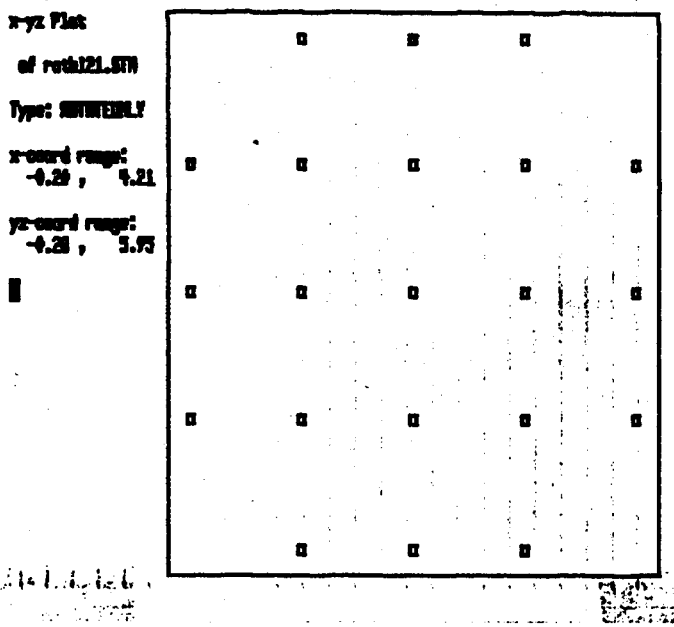

Fig. 8a - Location of antennas on a gridded version (ROTBL21) of a 21 antenna Azimuth-Rotation array projected on the x-y plane.

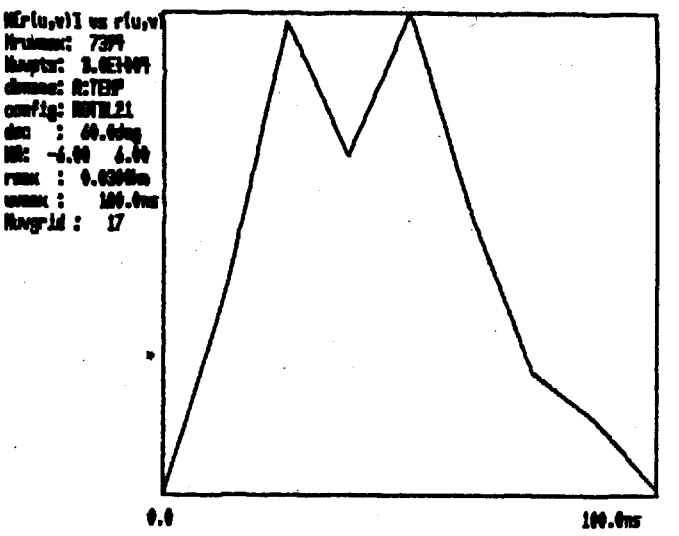

Fig. 8b - The distribution of data points in equal thickness rings in the u-v plane for a 60°, 12 hour observation with ROTBL21.

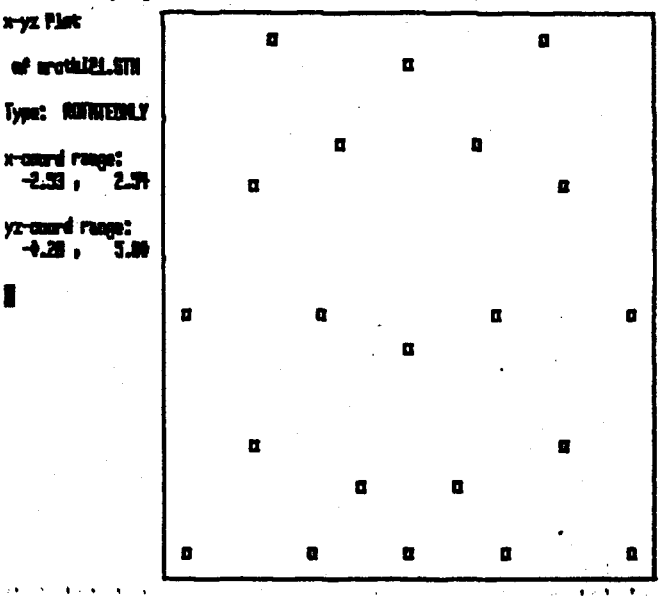

Fig. 8c - Location of antennas on a randomized version (MROTBL21) of a 21 antenna Azimuth-Rotation array projected on the x-y plane.

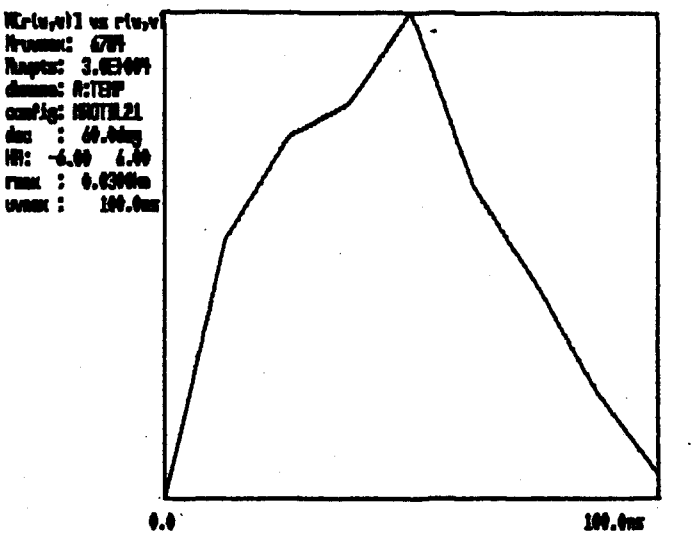

Fig. 8d - The distribution of data points in equal thickness rings in the u-v plane for a 60°, 12 hour observation with MROTBL21.

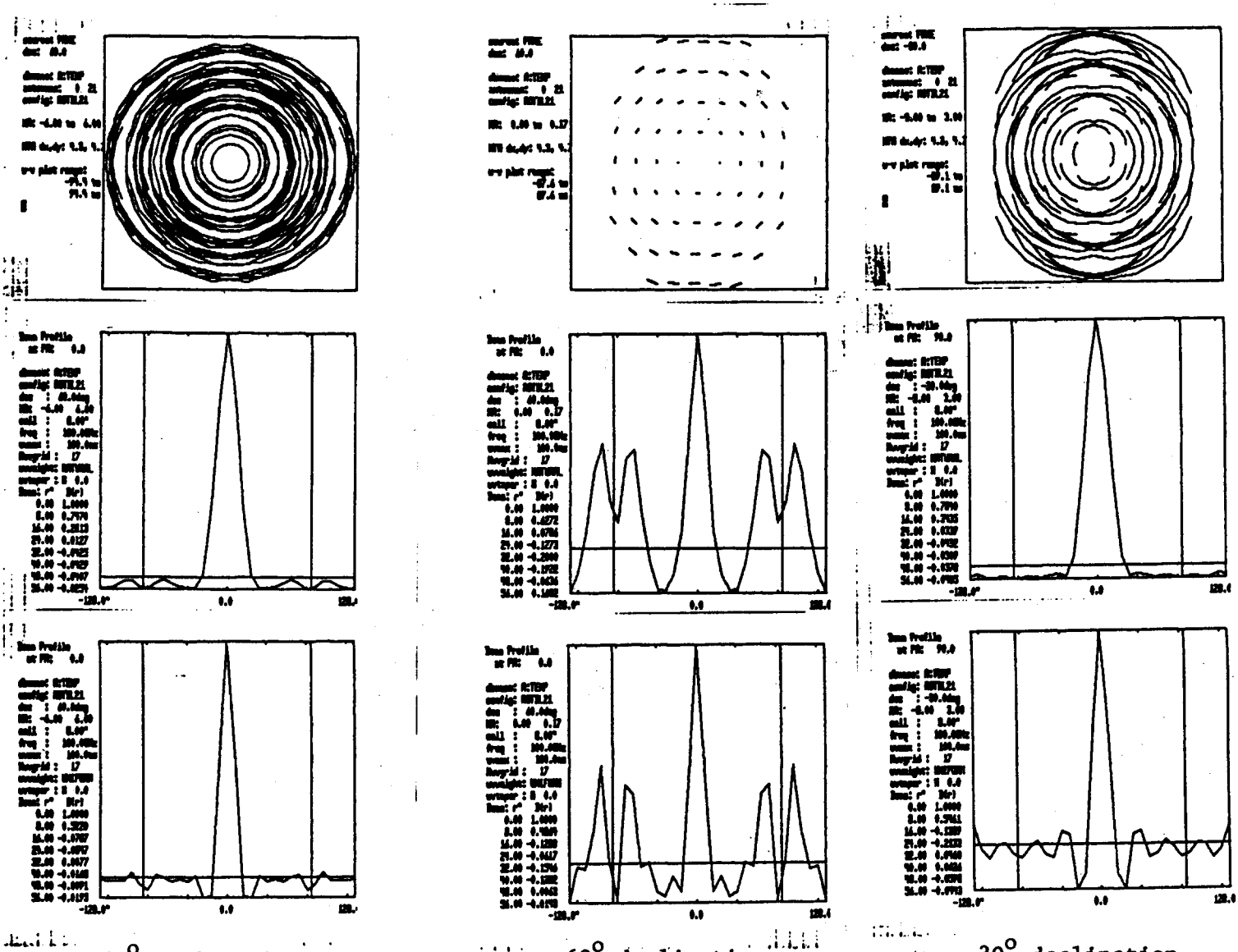

60° declination
-6h, 6h observation

60° declination
0h, 0.17h observation

-30° declination
-3h, 3h observation

Fig. 9 - The u-v plane coverage, and natural and uniform weighted beam profiles for three observing situations for the two-dimensional Azimuth-Rotation array ROTBL21.

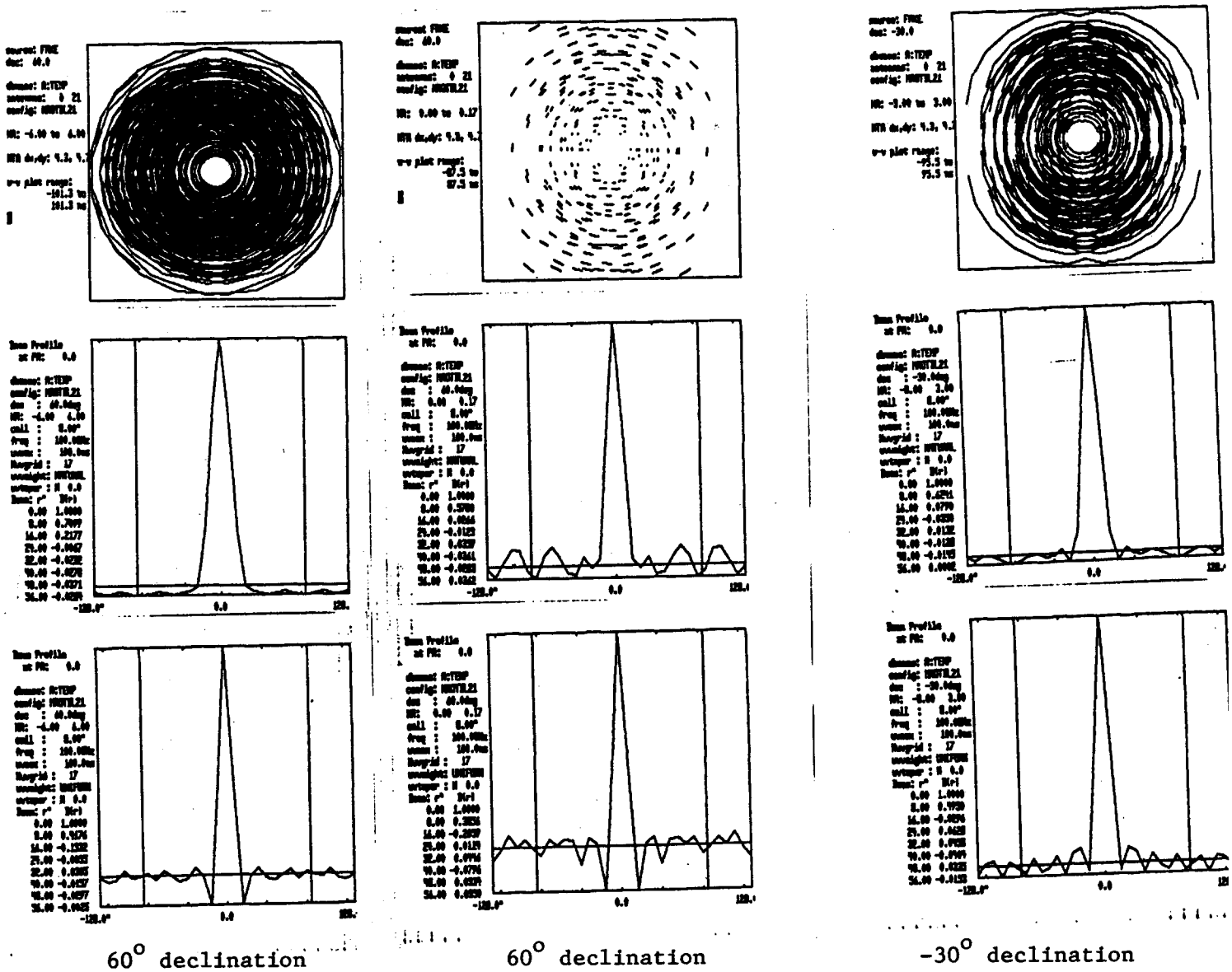

60° declination
-6h, 6h observation

60° declination
0h, 0.17h observation

-30° declination
-3h, 3h observation

Fig. 10 - The u-v plane coverage, and natural and uniform weighted beam profiles for three observing situations for the two-dimensional Azimuth-Rotation array MROTBL21.

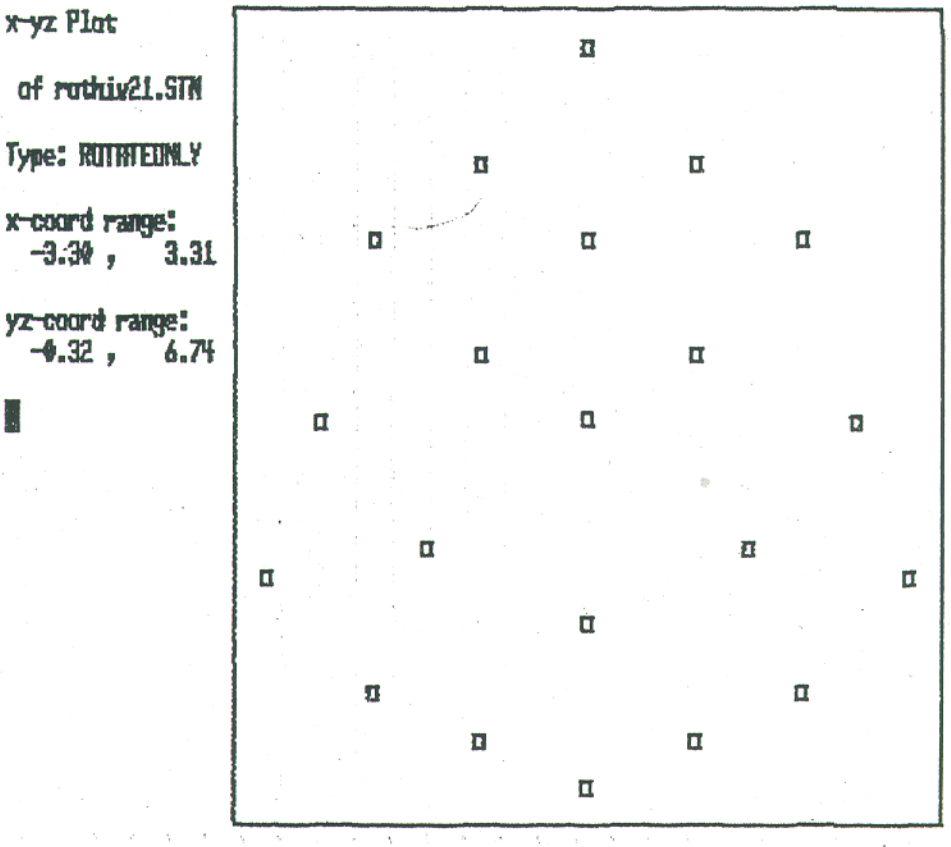

Fig. 11a- Location of antennas, as projected on the x-y plane, for 21 antennas mounted on the three-dimensional Azimuth-Rotation array ROTHIV21.

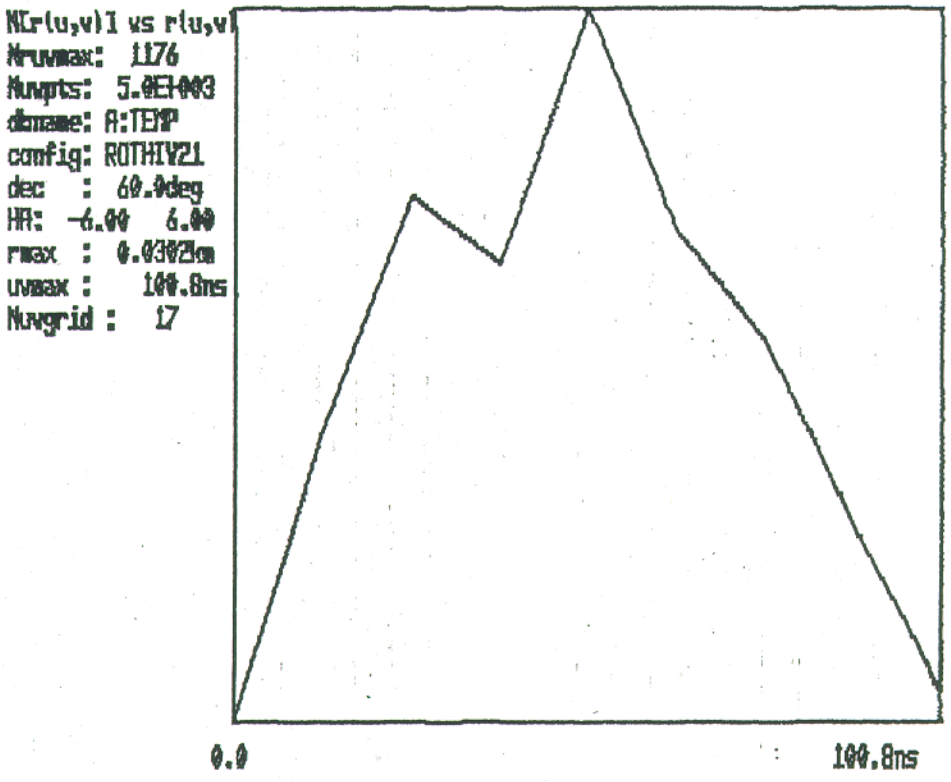

Fig. 11b - The distribution of data points in equal thickness rings in the u-v plane for a 60^{o}, 12 hour observation with the three-dimensional Azimuth-Rotation array ROTHIV21.

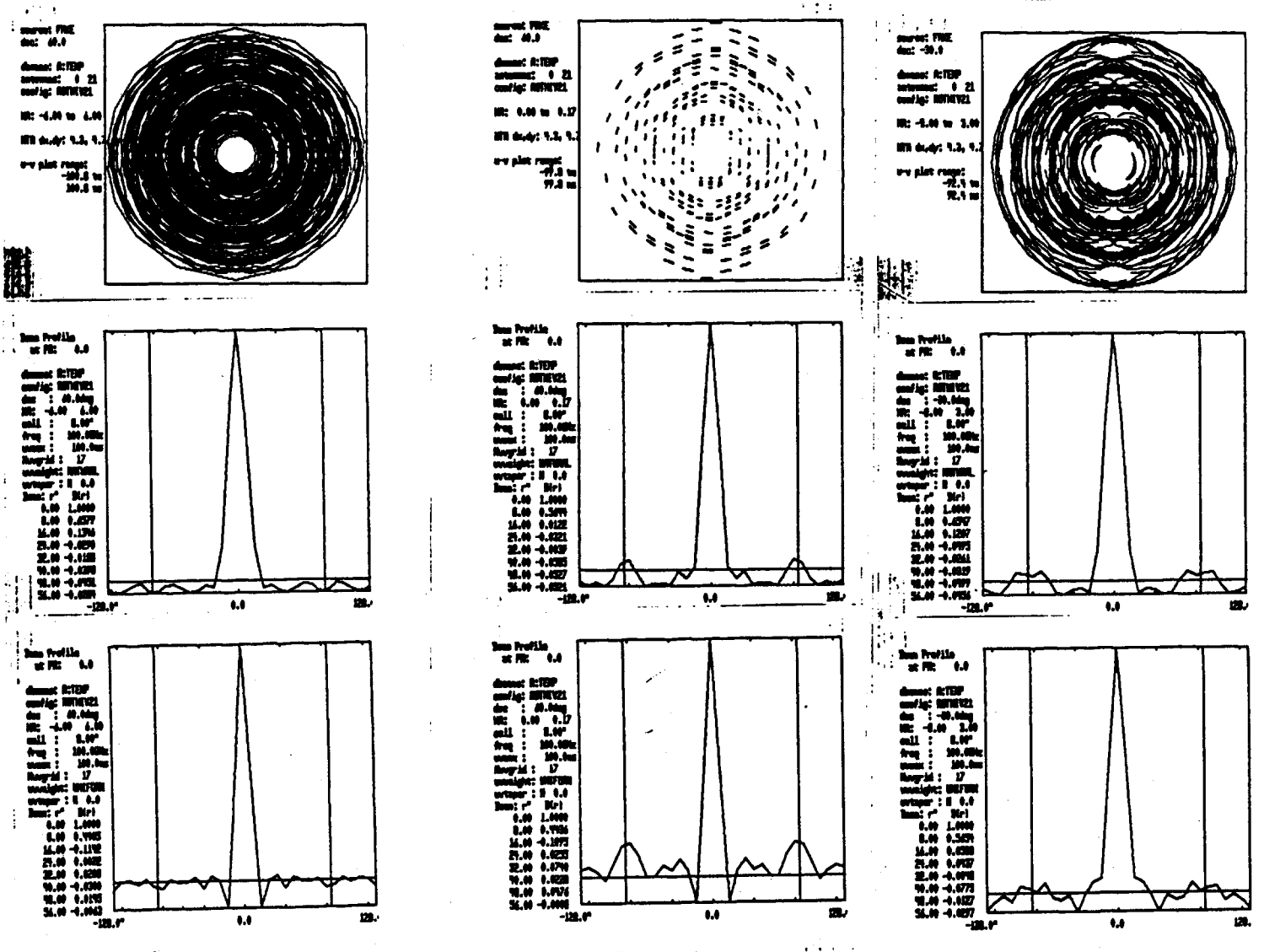

60° declination
-6h, 6h observation

60° declination
0h, 0.17h observation

-30° declination
-3h, 3h observation

Fig. 12 - The u-v coverage, and natural and uniform weighted beam profiles for three observing situations for the three-dimensional Azimuth-Rotation array ROTHIV21.